

# More about a successful vector-tensor theory of gravitation

R. Dale,<sup>a,1</sup> D. Sáez<sup>b,c</sup>

<sup>a</sup>Departamento de Estadística, Matemática e Informática, Universidad Miguel Hernandez, Elche, Alicante, Spain

<sup>b</sup>Departamento de Astronomía y Astrofísica, Universidad de Valencia, Burjassot, Valencia, Spain

<sup>c</sup>Observatorio Astronómico, Universidad de Valencia, E-46980 Paterna, Valencia, Spain

E-mail: [rdale@umh.es](mailto:rdale@umh.es), [diego.saez@uv.es](mailto:diego.saez@uv.es)

**Abstract.** The vector-tensor (VT) theory of gravitation revisited in this article was studied in previous papers, where it was proved that VT works and deserves attention. New observational data and numerical codes have motivated further development which is presented here. New research has been planned with the essential aim of proving that current cosmological observations, including Planck data, baryon acoustic oscillations (BAO), and so on, may be explained with VT, a theory which accounts for a kind of dark energy which has the same equation of state as vacuum. New versions of the codes CAMB and COSMOMC have been designed for applications to VT, and the resulting versions have been used to get the cosmological parameters of the VT model at suitable confidence levels. The parameters to be estimated are the same as in general relativity (GR), plus a new parameter  $D$ . For  $D = 0$ , VT linear cosmological perturbations reduces to those of GR, but the VT background may explain dark energy. The fits between observations and VT predictions lead to non vanishing  $|D|$  upper limits at the  $1\sigma$  confidence level. The value  $D = 0$  is admissible at this level, but this value is not that of the best fit in any case. Results strongly suggest that VT may explain current observations, at least, as well as GR; with the advantage that, as it is proved in this paper, VT has an additional parameter which facilitates adjustments to current observational data.

**Keywords:** Gravitation, Cosmology:theory, Cosmology: cosmological parameters, Cosmology: large scale structure of universe, Cosmology: microwave background radiation, Methods: numerical

---

<sup>1</sup>Corresponding author.

---

## Contents

<b>1</b>	<b>Introduction</b>	<b>1</b>
<b>2</b>	<b>Differential cosmological equations and initial conditions for integration</b>	<b>2</b>
2.1	On the codes VT-CAMB and VT-COSMOMC	6
<b>3</b>	<b>Estimating the parameters of the VT cosmological mode</b>	<b>7</b>
3.1	On the cosmological parameters	7
3.2	Fit models	8
<b>4</b>	<b>Results</b>	<b>9</b>
4.1	Planck+WP	9
4.2	Planck+WP+BAO	11
4.3	Planck+WP+SNIa	11
4.4	Planck+WP-TM	12
4.5	Planck+WP-TM-RSI	14
<b>5</b>	<b>Discussion and conclusions</b>	<b>18</b>

---

## 1 Introduction

In this paper, we are concerned with a vector-tensor theory of gravitation (hereafter VT). It involves two fields: the metric  $g^{\mu\nu}$  and the vector field  $A^\mu$ . This theory was studied in previous papers [1–4], in which it was proved that (i) there are no quantum ghosts and classical instabilities, (ii) the parametrized post-Newtonian limit is identical to that of general relativity (GR), (iii) the radius of the black hole horizon deviates with respect to that of GR, and the relative deviations may reach values close to 30 per cent, (iv) the energy density of the VT vector field plays the role of a cosmological constant, and (v) by using a minimal model -involving seven parameters- for the scalar perturbations of the cosmological background, the seven years WMAP (Wilkinson Map Anisotropy Probe) observations and accurate data about Ia supernova luminosities may be simultaneously explained. All this strongly suggests that VT deserves attention. This theory must be tested taking into account current observational data. Where appropriate, the reference [2] will be called paper I.

The field equations and the conservation laws of VT, as well as the basic equations describing the background universe and its perturbations were derived in [1, 2, 4]. Here, the VT foundations and equations are briefly summarized by using the following notation criteria: our signature is  $(-, +, +, +)$ , Latin (Greek) indexes run from 1 to 3 (0 to 3), symbol  $\nabla$  ( $\partial$ ) stands for a covariant (partial) derivative, the antisymmetric tensor  $F_{\mu\nu}$  is defined by the relation  $F_{\mu\nu} = \partial_\mu A_\nu - \partial_\nu A_\mu$ , quantities  $R_{\mu\nu}$ ,  $R$ , and  $g$  are the covariant components of the Ricci tensor, the scalar curvature and the determinant of the matrix  $g_{\mu\nu}$  formed by the covariant components of the metric, respectively. Units are chosen in such a way that the gravitational constant,  $G$ , and the speed of light,  $c$ , take on the values  $c = G = 1$ ; namely, we use geometrized units.

The VT action is [5, 6]:

$$I = \int (R/16\pi + \omega A_\mu A^\mu R + \zeta R_{\mu\nu} A^\mu A^\nu - \varepsilon F_{\mu\nu} F^{\mu\nu} + \gamma \nabla_\nu A_\mu \nabla^\nu A^\mu + L_m) \sqrt{-g} d^4x, \quad (1.1)$$

where  $\omega$ ,  $\zeta$ ,  $\gamma$ , and  $\varepsilon$  are dimensionless parameters. The values of  $\zeta$  and  $\gamma$  satisfy the condition  $\zeta = \gamma$ , parameter  $\omega$  vanishes, and the pair  $(\varepsilon, \gamma)$  satisfies the inequality  $2\varepsilon - \gamma > 0$ , which guarantees the absence of quantum ghosts and unstable modes in VT (see paper I and references cited therein). The inequality  $\gamma > 0$  must be also satisfied to have a positive  $A^\mu$  energy density -in the background universe- which will play the role of vacuum energy (see below). From these considerations, it follows that the inequalities  $\varepsilon > \frac{\gamma}{2} > 0$  must be satisfied. Moreover, as it was proved in [4], the parametrized post-Newtonian limits of VT and general relativity (GR) are identical whatever the values of the pair  $(\varepsilon, \gamma)$  may be. Tensor  $F_{\mu\nu}$  has nothing to do with the electromagnetic field [2, 4, 7].

The VT field equations derived from action (1.1) may be written as follows:

$$G^{\mu\nu} = 8\pi G(T_{GR}^{\mu\nu} + T_{VT}^{\mu\nu}), \quad (1.2)$$

$$2(2\varepsilon - \gamma)\nabla^\nu F_{\mu\nu} = J_\mu^A, \quad (1.3)$$

where  $J_\mu^A = -2\gamma\nabla_\mu(\nabla \cdot A)$  with  $\nabla \cdot A = \nabla_\mu A^\mu$ ,  $G^{\mu\nu}$  is the Einstein tensor,  $T_{GR}^{\mu\nu}$  is the GR energy momentum tensor, and

$$\begin{aligned} T_{VT}^{\mu\nu} = & 2(2\varepsilon - \gamma)[F^\mu_\alpha F^{\nu\alpha} - \frac{1}{4}g^{\mu\nu}F_{\alpha\beta}F^{\alpha\beta}] \\ & - 2\gamma[\{A^\alpha\nabla_\alpha(\nabla \cdot A) + \frac{1}{2}(\nabla \cdot A)^2\}g^{\mu\nu} \\ & - A^\mu\nabla^\nu(\nabla \cdot A) - A^\nu\nabla^\mu(\nabla \cdot A)]. \end{aligned} \quad (1.4)$$

Equation (1.3) leads to the following conservation law

$$\nabla^\mu J_\mu^A = 0 \quad (1.5)$$

for the fictitious current  $J_\mu^A$ . Moreover, the conservation laws  $\nabla_\mu T_{GR}^{\mu\nu} = 0$  and  $\nabla_\mu T_{VT}^{\mu\nu} = 0$  are satisfied by any solution of (1.2) and (1.3).

## 2 Differential cosmological equations and initial conditions for integration

The basic equations describing a flat homogeneous and isotropic background universe were derived [1, 2, 4] by using the basic VT equations of section 1, the Robertson-Walker line element

$$dS^2 = -dt^2 + a^2(dr^2 + r^2 d\theta^2 + r^2 \sin^2 \theta d\phi^2), \quad (2.1)$$

and a vector field with covariant components  $[A_{0B}(\tau), 0, 0, 0]$ . Here and hereafter,  $a$  is the scale factor, whose present arbitrary value is assumed to be  $a_0 = 1$ , symbol  $t$  ( $\tau$ ) stands for the coordinate (conformal) time, and the subscript  $B$  stands for background. Whatever the function  $f$  may be,  $f'$  and  $\dot{f}$  stand for the partial derivative with respect to the radial coordinate  $r$  and the conformal time  $\tau$ , respectively. Quantities  $\rho$  and  $p$  are the total density and pressure of the cosmological fluid. The subscripts  $b$ ,  $c$ ,  $\nu$ , and  $\gamma$  makes reference to the

baryon, cold dark matter, massless neutrinos, and photons, respectively, e.g.,  $\rho_\gamma$  is the CMB (cosmic microwave background) energy density. Finally, function  $\rho^A$  ( $p^A$ ) is the contribution to the energy density (pressure) corresponding to the vector field  $A^\mu$ .

As it was proved in papers [1, 2, 4], the following equations are satisfied:

$$3\frac{\dot{a}^2}{a^2} = 8\pi G a^2 (\rho_B + \rho_B^A) \quad (2.2)$$

$$-2\frac{\ddot{a}}{a} + \frac{\dot{a}^2}{a^2} = 8\pi G a^2 (p_B + p_B^A), \quad (2.3)$$

$$\rho_B^A = -p_B^A = \gamma \Xi_B^2, \quad (2.4)$$

where  $\Xi_B = (\nabla \cdot A)_B$ , and

$$\Xi_B = \text{constant} = -\frac{1}{a^2} [\dot{A}_{0B} + 2\frac{\dot{a}}{a} A_{0B}]. \quad (2.5)$$

These equations allow us to find functions  $a(\tau)$ ,  $A_{0B}(\tau)$  and  $\rho_B(\tau)$ , by using an appropriate equation of state for the cosmological fluid and suitable initial conditions (see below).

According to eqs. (2.4) and (2.5), for  $\gamma > 0$ , the positive energy density  $\rho_B^A$  has the same properties as the vacuum energy  $\rho_V$ . By this reason, we hereafter write  $\rho_B^A \equiv \rho_V$ . Moreover, eq. (2.4) allows us to write the constant  $\Xi_B$  in terms of other constants; so, one finds

$$\Xi_B = S_{gn} \left( \frac{\rho_V}{\gamma} \right)^{1/2}, \quad (2.6)$$

where  $S_{gn}$  only can take on the values +1 or -1.

For a given value of  $\Xi_B$  and suitable initial conditions for  $A_{0B}$ , eq. (2.5) may be numerically solved together with eqs. (2.2) and (2.3). All the initial conditions are taken, in the radiation dominated era, at  $z_{in} = 10^8$ . At this redshift, one easily obtains (see paper I) the following initial values of  $\tau$  and  $A_{0B}$

$$\tau_{in} = \left( \frac{\dot{a}}{a} \right)_{in}^{-1}, \quad (A_{0B})_{in} = -\frac{\Xi_B}{5(1+z_{in})^2} / \left( \frac{\dot{a}}{a} \right)_{in}. \quad (2.7)$$

The ratio  $(\dot{a}/a)_{in}$  may be calculated from eq. (2.2) as in the standard model with vacuum energy  $\rho_V$ ; hence, this ratio is that obtained by the code CAMB [8] for standard GR cosmology, which depends on the number of relativistic species contributing to  $\rho_{Bin}$ .

CAMB equations for the standard background with cosmological constant are valid in VT; however, in this last theory parameters  $S_{gn}$  and  $\gamma$  and the new background equation (2.5) must be included.

Let us now consider tensor, vector and scalar perturbations of the VT background universe, which were studied in [1, 2] by using the Bardeen formalism, in which  $Q^{(0)}$ ,  $Q_i^{(1)\pm}$ , and  $Q_{ij}^{(2)}$  are harmonics (see [1, 9, 10]) that may be used to expand the scalar, vector and tensor perturbations, respectively.

The covariant components  $A_\mu$  may be expanded in vector [superscript (1)] and scalar [superscript (0)] harmonics as follows:

$$A_\mu = (A_{0B} + \alpha^{(0)} Q^{(0)}, \beta^{(0)} Q_i^{(0)} + \alpha^{(1)\pm} Q_i^{(1)\pm}). \quad (2.8)$$

Evidently, there are no tensor modes in the  $A^\mu$  expansion. Therefore, in GR and VT there are the same tensor cosmological perturbations (primordial gravitational waves) evolving in the same way. The fundamental equation for these perturbations is

$$\ddot{H}_T^{(2)} + 2\frac{\dot{a}}{a}\dot{H}_T^{(2)} + k^2 H_T^{(2)} = p_B a^2 \Pi_T^{(2)} , \quad (2.9)$$

where  $\Pi_T^{(2)} Q_{ij}^{(2)}$  and  $H_T^{(2)} Q_{ij}^{(2)}$  (see [9]) are the tensor parts of the anisotropic stress tensor and the metric, respectively.

The vector modes  $A^{(1)\pm}$  satisfy the harmonic oscillator equation

$$\ddot{A}^{(1)\pm} + k^2 A^{(1)\pm} = 0 , \quad (2.10)$$

whose solutions are well known. Evidently, these vector modes are not coupled to the remaining modes of VT, which coincide with those of GR and evolve in the same way due to the fact that, according to eq. (1.4), the vector part of  $T_{VT}^{\mu\nu}$  vanishes.

All the scalar modes of GR are also involved in VT, but new scalar modes characteristic of VT must be included. The modes  $\alpha^{(0)}$  and  $\beta^{(0)}$  of eq. (2.8) are not appropriate. As it was proved in [1, 2], the most suitable VT scalar mode may be defined as follows:

$$\Xi \equiv \nabla \cdot A = \Xi_B (1 + \Xi Q^{(0)}) , \quad (2.11)$$

which means that the new VT mode is the first order term in the harmonic expansion of the scalar function  $\nabla \cdot A$ . There are no more independent VT scalar modes associated to field  $A^\mu$ .

Calculations are performed in the synchronous gauge; in which, the scalar perturbations corresponding to the metric, the four-velocity, and the energy-momentum tensor of a cosmological fluid are expanded as follows [11]:

$$\begin{aligned} g_{00} &= -a^2, & g_{0i} &= 0, \\ g_{ij} &= a^2 \left[ \left( 1 + \frac{h}{3} Q^{(0)} \right) \delta_{ij} - (h + 6\eta) Q_{ij}^{(0)} \right] \\ U_i &= \frac{a}{k} \theta Q_i^{(0)}, & \rho &= \rho_B (1 + \delta Q^{(0)}) \\ T_{ij} &= p_B (1 + \pi_L Q^{(0)}) \delta_{ij} + \frac{3}{2} (\rho_B + p_B) \sigma Q_{ij}^{(0)} , \end{aligned} \quad (2.12)$$

where function  $Q^{(0)} = \exp(i\vec{k} \cdot \vec{r})$  is a plane wave,  $Q_i^{(0)} = (-1/k) \partial_i Q^{(0)}$ , and  $Q_{ij}^{(0)} = k^{-2} \partial_j \partial_i Q^{(0)} + (1/3) \delta_{ij} Q^{(0)}$ . These expansions involve the independent functions  $h$ ,  $\eta$ ,  $\delta$ ,  $\theta$ ,  $\sigma$ , and  $\Xi$ , which depends on  $k$  and  $\tau$ . For adiabatic perturbations, functions  $\pi_L$  and  $\delta$  are not independent since they must satisfy the relation  $\pi_L = (\rho_B/p_B)(dp_B/d\rho_B)\delta$ .

Finally, quantities  $\delta$ ,  $\theta$  and  $\sigma$  may be calculated by using the following formulas [11]

$$\rho_B \delta = \sum_i \rho_{Bi} \delta_i , \quad (2.13)$$

$$(\rho_B + p_B) \theta = \sum_i (\rho_{Bi} + p_{Bi}) \theta_i , \quad (2.14)$$

$$(\rho_B + p_B) \sigma = \sum_i (\rho_{Bi} + p_{Bi}) \sigma_i , \quad (2.15)$$

where the subscript  $i$  run over the particle species ( $b, c, \nu, \gamma$ ).

Let us now summarize the evolution equations of the above scalar modes, which were derived in [1, 2, 11] by using the above expansions and the VT equations.

The  $\Xi$  evolution is governed by a second order differential equation [1, 2], which is equivalent to the following system of two first order differential equations:

$$\dot{\Xi} = \xi \quad (2.16)$$

$$\dot{\xi} = -2\frac{\dot{a}}{a}\xi - k^2\Xi ; \quad (2.17)$$

these equations do not involve the modes of GR, but only the VT quantity  $\xi$ , the wavenumber, and quantities related to the background. This fact is very advantageous eqs. (2.16) and (2.17) are included into CAMB for adaptation to VT estimates.

In the chosen gauge, the following linearized equations are also satisfied:

$$k^2\eta - \frac{1}{2}\frac{\dot{a}}{a}\dot{h} = 4\pi G[-a^2\rho_B\delta - 2\gamma\Xi_B(a^2\Xi_B\Xi + A_{0B}\xi^{(0)})] \quad (2.18)$$

$$k^2\dot{\eta} = 4\pi G[a^2(\rho_B + p_B)\theta + 2\gamma k^2 A_{0B}\Xi_B\Xi] \quad (2.19)$$

$$\ddot{h} + 2\frac{\dot{a}}{a}\dot{h} - 2k^2\eta = -24\pi G[a^2 p_B \pi_L - 2\gamma\Xi_B(a^2\Xi_B\Xi - A_{0B}\xi)] \quad (2.20)$$

$$\ddot{h} + 6\ddot{\eta} + 2\frac{\dot{a}}{a}(\dot{h} + 6\dot{\eta}) - 2k^2\eta = -24\pi G a^2(\rho_B + p_B)\sigma . \quad (2.21)$$

The terms involving  $\gamma$  are the VT corrections to the standard GR equations (21a)–(21d) derived in [11], which are formally recovered for  $\gamma = 0$ . These terms –appearing only in VT cosmology– have been included in CAMB; they have been proved to be independent of both  $S_{gn}$  and  $\gamma$ .

Since the energy-momentum conservation law  $\nabla_\alpha T_{GR}^{\alpha\beta} = 0$  is satisfied (as in GR), the variables  $\delta_\gamma, \delta_\nu, \theta_\gamma, \theta_\nu$  and  $\sigma_\nu$  obey the same equations as in GR cosmology and, consequently, we can write (see eqs. (92) in paper [11]):

$$\begin{aligned} \dot{\delta}_\gamma + \frac{4}{3}\theta_\gamma + \frac{2}{3}\dot{h} &= 0, & \dot{\theta}_\gamma - \frac{1}{4}k^2\delta_\gamma &= 0, \\ \dot{\delta}_\nu + \frac{4}{3}\theta_\nu + \frac{2}{3}\dot{h} &= 0, & \dot{\theta}_\nu - \frac{1}{4}k^2(\delta_\nu - 4\sigma_\nu) &= 0, \\ \dot{\sigma}_\nu - \frac{2}{15}(2\theta_\nu + \dot{h} + 6\dot{\eta}) &= 0 . \end{aligned} \quad (2.22)$$

The Thompson interaction between photons and electrons (including reionization) is not affected by the presence of the vector field  $A^\mu$  and, consequently, the CAMB treatment of this scattering is not to be modified.

Finally, as it was proved in paper I, the initial conditions for the VT scalar modes, at redshift  $z_{in} = 10^8$  (radiation dominated era), are the following:

$$\begin{aligned}
h &= C(k\tau)^2 + \tilde{C}(k\tau)^4, \quad \delta_\gamma = \delta_\nu = \frac{4}{3}\delta_b = \frac{4}{3}\delta_c = -\frac{2}{3}h, \\
\theta_c &= 0, \quad \theta_\gamma = \theta_b = -\frac{1}{18}Ck^4\tau^3 - \frac{1}{30}\tilde{C}k^6\tau^5, \\
\theta_\nu &= -\frac{23 + 4R_\nu}{18(15 + 4R_\nu)}Ck^4\tau^3 - \frac{1}{30}\tilde{C}k^6\tau^5, \\
\sigma_\nu &= \frac{4}{3(15 + 4R_\nu)}Ck^2\tau^2, \quad \Xi = Dk^4, \quad \xi = \dot{\Xi} = 0, \\
\eta &= \left[2 - \frac{5 + 4R_\nu}{6(15 + 4R_\nu)}(k\tau)^2\right]C,
\end{aligned} \tag{2.23}$$

where  $D = 3(1 + z_{in})^2\tilde{C}/[8\pi G\rho_V(\dot{a}/a)_{in}^2]$ ; hence, these formulas involve two independent normalization constants  $C$  and  $D$  (or  $C$  and  $\tilde{C}$ ) and the quantity  $R_\nu = \rho_{\nu B}/(\rho_{\nu B} + \rho_{\gamma B})$ . Constant  $C$  must be fixed as in GR to guarantee that VT perturbations reduce to those of GR as  $D$  (constant  $D_1$  in paper I) tends to zero.

In the study performed in paper I, which was based on the differential equations and initial conditions summarised in this section, the following important numerical results were found:

1) For spatial scales  $L \gtrsim 2800h^{-1} \text{ Mpc}$ , the VT quantities  $\dot{h}$  and  $\dot{\eta}$  are almost identical to those of GR for any redshift  $z$ ; however, for  $L \lesssim 2800h^{-1} \text{ Mpc}$ , the VT values of  $\dot{h}$  and  $\dot{\eta}$  deviate significantly from the GR values for  $z \lesssim 5$ . The resulting deviations involve oscillations. Since quantities  $\dot{h}$  and  $\dot{\eta}$  are explicitly involved in the equations describing the evolution of the photon distribution function (see eq. (63) in [11]), their deviations - with respect to GR- must leave imprints on the CMB temperature angular power spectrum; however, these deviations should not affect CMB polarization, which is essentially generated during recombination ( $z \sim 1100$ ). This fact was numerically verified in paper I.

2) For  $\ell \gtrsim 250$  ( $\ell \lesssim 5$ ) the  $C_\ell$  multipoles of GR and VT are almost identical (very similar); hence, the angular power spectrum of VT only deviates -significantly- with respect to that of GR for  $5 \lesssim \ell \lesssim 250$ . The deviations depend on  $|D|$ , but they are independent of the sign of  $D$ .

As it is pointed out below, these results have been very useful to properly modify the codes CAMB and COSMOMC [12] for VT applications.

## 2.1 On the codes VT-CAMB and VT-COSMOMC

It is worthwhile to describe some changes, which have been necessary to built up VT-CAMB starting from CAMB. All these changes are suggested by the outcomes summarized in section 2. The basic VT cosmological equations and initial conditions -at  $z_{in} = 10^8$ - must be implemented in VT-CAMB as it has been discussed in the aforementioned section; nevertheless, other changes -in CAMB- are also necessary to ensure high enough accuracy in VT-CAMB predictions. The most important of these changes is now described.

The code CAMB estimates some integrals along the background null geodesics -until vanishing redshift- to get the CMB temperature and polarization anisotropy. Since it has been emphasized in section 2 that VT and GR are almost equivalent at  $z > 5$ , and also that the deviations arising at  $z \lesssim 5$  involve oscillations. It is evident that many integration steps must be included in the redshift interval  $(0, \sim 5)$  to properly take into account the deviations

between VT and GR. We have estimated the minimum number of integration steps leading to satisfactory results. More steps are not necessary since they do not improve on the results. In the original CAMB code, the number of steps in the interval  $(0, \sim 5)$  is not sufficient for VT applications.

The COSMOMC version we have modified uses the so-called *nuisance* parameters, which have been defined to take into account -in the context of Planck experiment- contaminant foregrounds, beam structure, and so on; hence, the treatment of Planck data cannot be realized with COSMOMC versions designed to deal only with WMAP data (old versions as that modified in paper I). Modifications necessary to get VT-COSMOMC are simple; this code calls VT-CAMB and includes the new parameter  $D$  to be adjusted.

If the code VT-CAMB is used for  $D = 0$ , results are not identical to those of the original CAMB, which is due to the fact that, even for  $D = 0$ , the number of integration time steps used by CAMB and VT-CAMB are very different. It has been verified that the differences between these two codes are negligible for  $D = 0$ , which means that the original CAMB code is accurate enough for the standard GR cosmological model (hereafter GR-CM), and no more time steps are necessary.

### 3 Estimating the parameters of the VT cosmological mode

In general, parameter estimates require: (i) accurate enough observational data for an appropriate set of observable quantities, (ii) a numerical code predicting the values of these observable quantities for given values of appropriate cosmological parameters; e.g., CAMB is a code of this kind, which has been designed to work in the framework of GR-CM, and (iii) another numerical code based on suitable statistical methods as, e.g., Markov chains, which allows us to fit current observational data and numerical predictions. A code of this type is COSMOMC, which was designed to work in the GR-CM.

#### 3.1 On the cosmological parameters

The following basic assumptions are maintained all along the paper: the background universe is flat, perturbations are adiabatic, the dark energy equation of state is  $p = W\rho$  with  $W = -1$ , vector modes are negligible, the mean CMB temperature is  $T_{CMB} = 2.726$ , and the effective number of relativistic species is 3.046.

At horizon crossing, the power spectrum of the scalar energy density perturbations is parametrized as follows:

$$P_s(k) = A_s \left( \frac{k}{k_0} \right)^{n_s - 1 + (1/2)(dn_s/d \ln k) \ln(k/k_0)}, \quad (3.1)$$

whereas the power spectrum of the gravitational wave amplitudes is of the form

$$P_t(k) = A_t \left( \frac{k}{k_0} \right)^{n_t}. \quad (3.2)$$

The pivot scale is  $k_0 = 0.05 \text{ Mpc}^{-1}$ . It is usual to define the parameter  $r_{0.05} = A_t/A_s$ , which depends on  $n_t$  in most relevant cases; e.g., in inflationary models based on a scalar field, the so-called consistency condition for slow-roll inflation,  $r_{0.05} = -n_T/8$ , is satisfied. Since this condition is assumed here, as it is done in [13], the free independent parameters involved in eqs. (3.1)-(3.2) are  $A_s$ ,  $r_{0.05}$ ,  $n_s$ , and  $dn_s/d \ln k$ , which are the normalization constant of  $P_s(k)$ , the primordial tensor to scalar ratio, the spectral index of  $P_s(k)$ , and the running



index, respectively. Sometimes, for comparisons with [13], we use the parameter  $r_{0.002}$ , which is defined as  $r_{0.05}$ , but assuming the pivot scale  $k_0 = 0.002 \text{ Mpc}^{-1}$ .

The six parameters used to fit predictions and observations in the GR-CM (minimal fit model) are  $\Omega_b h^2$ ,  $\Omega_c h^2$ ,  $\tau$ ,  $n_s$ ,  $\log[10^{10} A_s]$ , and  $\theta_{MC}$ , where  $\Omega_b$  and  $\Omega_c$  are the density parameters of baryons and dark matter, respectively,  $h$  is the reduced Hubble constant,  $\tau$  is the reionization optical depth, and the parameter  $\theta_{MC}$  (angular acoustic scale) is the ratio  $r_s(z_*)/d_A(z_*)$ , where  $r_s(z_*)$  is the sound horizon at decoupling redshift  $z_*$  and  $d_A(z_*)$  is the angular diameter distance for the same redshift.

All the parameters involved in standard GR cosmology are also parameters of the VT cosmological model (hereafter VT-CM); nevertheless, in the VT case, there is an additional parameter denoted  $D$  (see section 2).

The minimal fit model (for VT-CM), used here and also in paper I, involves the six parameters of the minimal GR-CM fit plus  $D$ .

### 3.2 Fit models

Various fits have been considered -in this paper- to study the VT-CM viability. They improve on the fit used in paper I to estimate cosmological parameters in VT-CM. The main differences between the five fit models of this paper and the fit approach of paper I are now pointed out.

The fit method of paper I was designed as follows: (a) the seven cosmological parameters of the minimal fit (see above) were assumed, (b) appropriate versions of codes CMBFAST [14] and COSMOMC (january 2012 version) were modified and coupled with the essential aim of estimating the seven chosen parameters, (c) vector and tensor modes were not considered at all to do predictions, and (d) only data about Ia supernovae (SNIa) and WMAP7 CMB anisotropies were taken into account.

For comparisons, let us describe the five fit models analyzed in this paper. They are all based on the use of the VT-CAMB and VT-COSMOMC numerical codes, which are adaptations of original CAMB and COSMOMC versions (december 2013), specially designed -by us- to be applied in the case  $D \neq 0$ .

Let us now focus our attention on the features of the five fit models we have selected:

In the first fit, we use the same cosmological parameters and perturbation modes as in the approach of paper I (see above); however, the updated (december 2013) data sets are Planck CMB anisotropies (Planck), and WMAP polarization anisotropy at low  $\ell \lesssim 23$  (WP). Following a notation similar to that of Planck papers [13], this fit is hereafter named Planck+WP

Our second (third) fit is like Planck+WP, but it also consider updated BAO (SNIa) information; hence, it is named Planck+WP+BAO (Planck+WP+SNIa)

The fourth fit model includes the same data sets as Planck+WP, plus primordial gravitational waves (tensor modes  $\equiv$  TM). The additional parameter  $r_{0.05}$  is then necessary. This model is hereafter called Planck+WP-TM

Finally, the fifth fit is like Planck+WP-TM, but an additional parameter  $dn_s/d\ln k$  is included to analyze the effects of a running spectral index (RSI) with a weak dependence on  $k$ . This fit is named Planck+WP-TM-RSI.

Since we are particularly interested in possible differences between GR-CM and VT-CM, parameters related with particle interactions as, e.g., the total neutrino mass  $\sum m_\nu$  (summed over the three neutrino families), the effective neutrino number  $N_{eff}$  (relativistic particles), and so on (see [13, 15, 16]), are not considered in our fits. This procedure is qualitatively justified by the fact that the CMB anisotropy due to physical interactions among particles must

be produced inside the effective horizon at  $z \gtrsim 1100$ , namely, at angular scales corresponding to  $\ell \gtrsim 220$  (in a flat universe), which means that no important effects are expected at  $\ell \lesssim 100$ ; namely, at the angular scales producing the most important deviations between VT and GR. As an additional result of these considerations, high  $\ell$  data from SPT (South Pole Telescope) and ACT (Atacama Cosmology Telescope) small scale CMB experiments should not produce relevant differences between GR-CM and VT-CM and, consequently, this high  $\ell$  information is not considered in our fits.

## 4 Results

A systematic comparison of the parameters obtained for  $D = 0$  (GR-CM) and  $D \neq 0$  (VT-CM) has been performed for the five fit models described above, in each of them, codes VT-CAMB and VT-COSMOMC are used both for  $D = 0$  and for  $D \neq 0$ . Whatever the fit may be, parameters different from  $D$  and observational data are the same for both  $D = 0$  and  $D \neq 0$ ; in this way, differences between GR-CM ( $\Lambda$ CDM) and VT-CM are properly estimated.

Planck collaboration has developed an exhaustive study to estimate the cosmological parameters -by using CAMB and COSMOMC- in the context of GR-CM [13]. Some feasible comparisons between our VT-CM results and those of the Planck team (GR-CM) are presented.

Let us now present our results and comparisons for the chosen fit models.

### 4.1 Planck+WP

Results corresponding to this fit, for  $D = 0$  (GR) and for  $D \neq 0$ , are compared in Table 1 and figures 1 and 2.

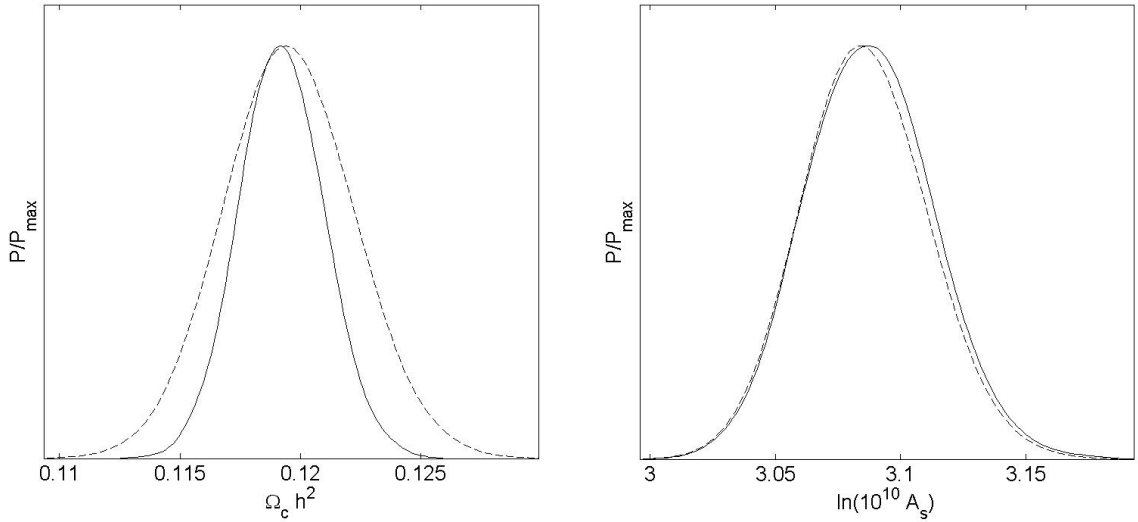
The first column shows fourteen parameters. The first seven of them (above the horizontal line) are the fitted parameters in VT, and the remaining ones are given by CAMB as derived parameters. The second, third and fourth columns display, in VT, the best fit (BF) values, the lower (L1) limit at  $1\sigma$  confidence level, and the corresponding upper (U1) limit, respectively. For comparison with the results obtained in GR, the relative deviations  $\Delta(L1) = 2[L1(VT) - L1(GR)]/[L1(VT) + L1(GR)]$  and  $\Delta(U1) = 2[U1(VT) - U1(GR)]/[U1(VT) + U1(GR)]$  are presented in the fifth and sixth columns, respectively. Finally the seventh column gives the ratio  $R1 = [U1(VT) - L1(VT)]/[U1(GR) - L1(GR)]$  between the amplitudes of the  $(U1, L1)$  intervals of VT and GR. All the Tables presented below have very similar structures, with small changes to be described in due time.

Since we have verified that results do not depend on the sign of  $D$  (see also paper I), from Table 1, it follows that, for positive (negative) values of  $D \times 10^{-8}$ , this quantity belongs to the interval  $[0, 2.149]$  ( $[-2.149, 0]$ ) with a probability  $\sim 68.2\%$  ( $1\sigma$ ). Parameter  $D$  -characteristic of VT- is also adjusted in other fits (see below). Results for different fits will be compared below to discuss the statistical role of  $|D|$ .

In the fifth and sixth columns, we see that the relative deviations -between VT and GR- measured by  $\Delta L1$  and  $\Delta U1$  are small for all the adjusted parameters. Parameters  $\tau$  and  $\Omega_c h^2$  undergo the maximum relative deviations, which are small in both cases since  $|\Delta L1|$  and  $|\Delta U1|$  do not exceed 1.46%. Finally, the seventh column shows that, at  $1\sigma$  level, the inequality  $R1 \geq 1$  is satisfied for the fourteen parameters, which means that, for every parameter, the amplitude of the interval  $(U1, L1)$  in VT is greater than in GR. This strongly suggests that a parameter  $D \neq 0$  facilitates the adjustments between predictions and cosmological observations.

**Table 1.** Planck+WP fit

Parameter	BF	L1	U1	$\Delta(L1)$	$\Delta(U1)$	R1
$D \times 10^{-8}$	1.596	0.000	2.149	-	-	-
$\Omega_b h^2$	0.02216	0.02179	0.02235	-0.27%	0.04%	1.143
$\Omega_c h^2$	0.1187	0.1169	0.1222	-0.51%	0.99%	1.514
$100\theta_{MC}$	1.0411	1.0407	1.0419	-0.01%	0.00%	1.091
$\ln(10^{10} A_s)$	3.085	3.060	3.110	-0.10%	-0.10%	1.000
$n_s$	0.9657	0.9535	0.9684	-0.18%	0.20%	1.319
$\tau$	0.0893	0.0749	0.1013	-1.46%	-0.88%	1.008
$\Omega_\Lambda$	0.697	0.677	0.710	-1.12%	0.59%	1.557
$\Omega_m$	0.303	0.290	0.323	-1.44%	2.38%	1.557
$\sigma_8$	0.838	0.827	0.853	-0.10%	0.13%	1.082
$z_{re}$	10.98	9.86	12.04	-0.81%	-0.66%	1.000
$H_0$	68.22	66.72	69.12	-0.82%	0.41%	1.529
$Y_P$	0.24488	0.24473	0.24496	-0.01%	0.00%	1.137
$t_0$	13.78	13.74	13.83	0.00%	0.07%	1.125

**Figure 1.** Marginalized distribution functions normalized to unity for the parameters  $\Omega_c h^2$  (left) and  $\ln(10^{10} A_s)$  (right). Continuous (dashed) lines correspond to GR (VT)

The same can be seen in figure 1, where the marginalized likelihood function  $P/P_{max}$  corresponding to VT (dashed line) is wider than that of GR (solid line) for the parameter  $\Omega_c h^2$  ( $R \simeq 1.5$  in Table 1); however, for  $\ln(10^{10} A_s)$ , having  $R1 \simeq 1$ , both likelihood functions are almost identical as it was expected. Also figure (2) displays the same situation; in fact, from inside out, red (black) curves show the  $1\sigma$ ,  $2\sigma$  and  $3\sigma$  limits for VT (GR). Moreover, in the left panel [pair  $(H_0, \Omega_m)$ ] as well as in the right panel [pair  $(\tau, \Omega_m)$ ], we see that -almost everywhere- the red curves are outside the corresponding black lines.

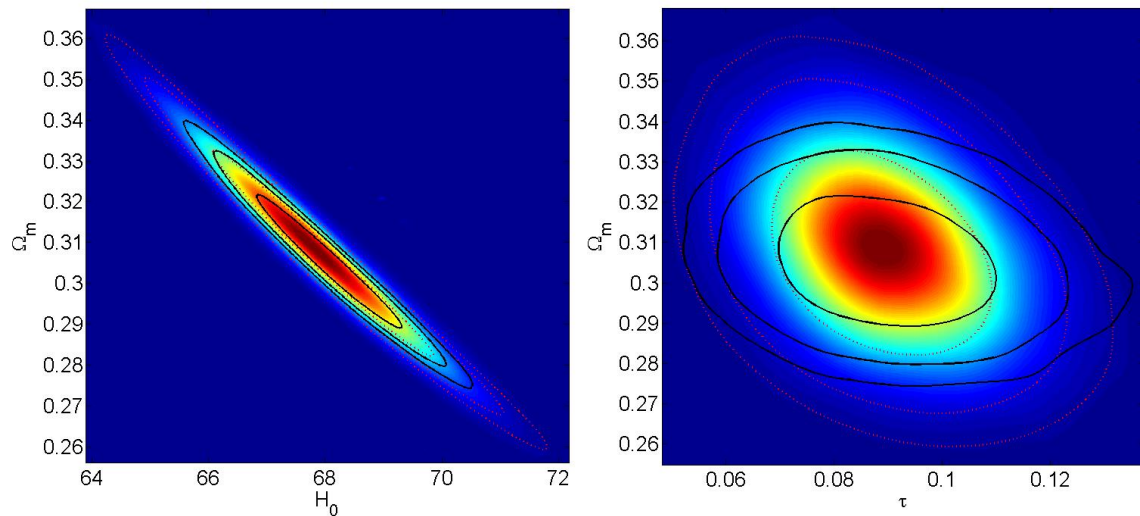


**Figure 2.** Marginalized distribution functions (color), for the pairs  $(H_0, \Omega_m)$  [left] and  $(\tau, \Omega_m)$  [right]. Red [black] contours correspond to the  $1\sigma$  (inner),  $2\sigma$  (middle) and  $3\sigma$  (outer) confidence levels in VT [GR].

## 4.2 Planck+WP+BAO

In this fit. Results for  $D = 0$  (GR) and for  $D \neq 0$  (VT) are compared in Table 2 and figure 3. From the Table it follows that, for all the parameters,  $|\Delta L1|$  and  $|\Delta U1|$  do not exceed 0.92% and  $R1$  is very close to unity. If these results are compared with those of the Planck+WP fit of section 4.1 (Table 1), we see that BAO data have reduced the differences between GR and VT at the  $1\sigma$  level for all the common parameters. From the left panel of figure 3, it follows that the solid (Planck+WP) and dashed (Planck+WP+BAO) lines are almost identical for  $D \times 10^{-8} \lesssim 0.4$  and for  $D \times 10^{-8} \gtrsim 1.7$ , which clearly explains that the best fit value of  $D \times 10^{-8}$  is as small as 0.316, and also that the  $1\sigma$  limit of parameter  $D \times 10^{-8}$  takes on the value 2.149, which is identical to that of the Planck+WP case. The  $1\sigma$  limit is a meaningful quantity; however, as it is commented in [13] (last paragraph of section 2), best fit values are not very numerically stable and should not be over-interpreted. The probabilities assigned in COSMOMC have numerical errors and, consequently, inside a flat enough region of the  $D$  distribution function, the maximum likelihood value of  $D$  could arise as a result of these errors; which makes this value unstable against the number of selected chains (convergence criterium). On account of these comments, best fits are hereafter interpreted with caution.

## 4.3 Planck+WP+SNIa

For this third fit, results corresponding to  $D = 0$  (GR) and  $D \neq 0$  (VT) may be compared with the help of Table 3 and figure 3. In this Table, one can see that, for all the parameters, quantities  $|\Delta L1|$  and  $|\Delta U1|$  do not exceed 0.5% and  $R$  is very close to unity. If these results are compared with those of the Planck+WP fit of section 4.1 (Table 1), we see that, as it occurs with BAO, SNIa data have also reduced the differences between GR and VT, at the  $1\sigma$  level, for all the parameters being common to both theories. For positive values, the  $1\sigma$  limit of  $D \times 10^{-8}$  takes on the value 2.245, which is a little greater than that of the Planck+WP case (2.149). This is in agreement with the fact that, in the left panel of figure 3, the dotted

**Table 2.** Planck+WP+BAO fit

Parameter	BF	L1	U1	$\Delta(L1)$	$\Delta(U1)$	R1
$D \times 10^{-8}$	0.316	0.000	2.149	-	-	-
$\Omega_b h^2$	0.02205	0.02184	0.02233	-0.05%	-0.04%	1.000
$\Omega_c h^2$	0.1190	0.1174	0.1209	-0.09%	0.00%	1.029
$100\theta_{MC}$	1.0412	1.0408	1.0419	0.00%	0.00%	1.000
$\ln(10^{10} A_s)$	3.067	3.060	3.110	-0.07%	-0.10%	0.980
$n_s$	0.9602	0.9559	0.9676	0.06%	0.09%	1.026
$\tau$	0.0795	0.0758	0.1016	-0.92%	-0.88%	0.992
$\Omega_\Lambda$	0.695	0.685	0.705	0.01%	0.07%	1.020
$\Omega_m$	0.305	0.295	0.315	-0.17%	-0.03%	1.020
$\sigma_8$	0.831	0.827	0.851	-0.07%	-0.09%	0.992
$z_{re}$	10.15	9.92	12.07	-0.60%	-0.74%	0.986
$H_0$	68.02	67.31	68.87	0.01%	0.06%	1.020
$Y_P$	0.24484	0.24475	0.24496	0.00%	0.00%	1.000
$t_0$	13.79	13.74	13.82	0.00%	0.00%	1.000

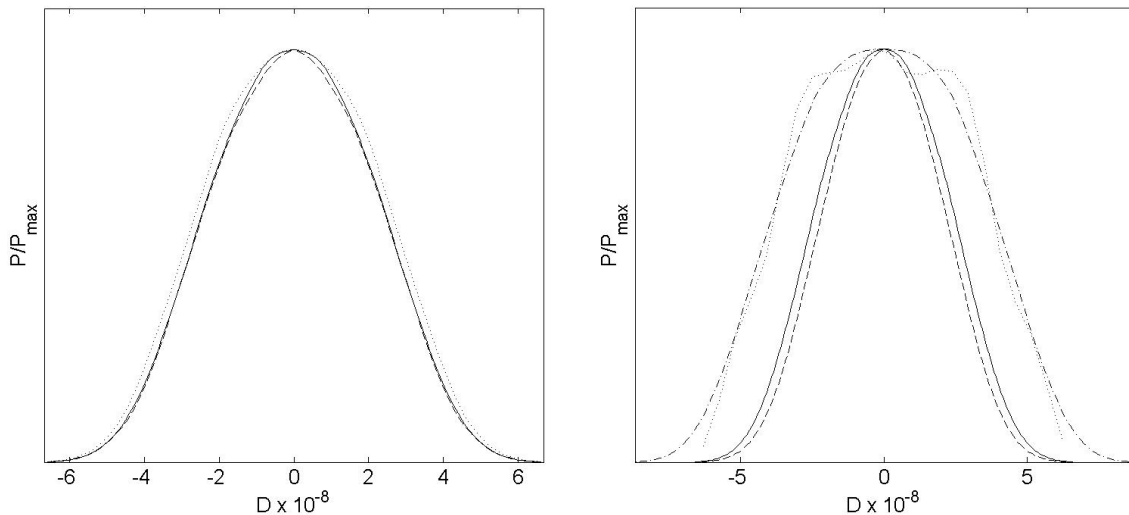


**Figure 3.** Marginalized distribution functions normalized to unity ( $P/P_{max}$ ) for the parameter  $D \times 10^{-8}$  in various fits. Left: solid, dashed, and dotted lines correspond to the Planck-WP, Planck-WP+BAO, and Planck-WP-SNIa, respectively. Right: pointed curve was obtained with WMAP and SNIa data in paper I, whereas solid, dashed, and dot-dashed lines give  $P/P_{max}$  in Planck-WP, Planck+WP-TM, and Planck+WP-TM-RSI, respectively

(Planck+WP+SNIa) line is a little wider than the solid (Planck+WP) curve. The best fit value of  $D \times 10^{-8}$  is 0.756, which is located in the flat central part of the dotted curve of figure 3; hence, this value is little meaningful (see section 4.2).

#### 4.4 Planck+WP-TM

The three VT fits considered in previous sections are minimal (seven parameters). Although minimal fits in GR-CM (six parameters) have led to very good results in the analysis of

**Table 3.** Planck+WP+SNIa fit

Parameter	BF	L1	U1	$\Delta(L1)$	$\Delta(U1)$	R1
$D \times 10^{-8}$	0.756	0.000	2.245	-	-	-
$\Omega_b h^2$	0.02208	0.02191	0.02246	0.03%	0.06%	1.012
$\Omega_c h^2$	0.1200	0.1154	0.1203	-0.21%	-0.21%	0.997
$100\theta_{MC}$	1.0414	1.0409	1.0421	0.00%	0.00%	1.000
$\ln(10^{10} A_s)$	3.097	3.060	3.125	-0.05%	-0.06%	0.994
$n_s$	0.9630	0.9577	0.9720	0.13%	0.16%	1.016
$\tau$	0.0930	0.0772	0.1043	-0.37%	-0.49%	0.991
$\Omega_\Lambda$	0.691	0.688	0.717	0.23%	0.19%	0.993
$\Omega_m$	0.309	0.283	0.312	-0.48%	-0.50%	0.993
$\sigma_8$	0.847	0.823	0.848	-0.13%	-0.13%	0.998
$z_{re}$	11.36	10.02	12.22	-0.33%	-0.35%	0.990
$H_0$	67.78	67.55	69.82	0.17%	0.15%	0.996
$Y_P$	0.24485	0.24477	0.24501	0.00%	0.00%	1.043
$t_0$	13.79	13.71	13.81	-0.07%	0.00%	1.111

WMAP [17, 18] and Planck [13, 19–21] data; extended fits with more parameters have been also considered [13, 22]. Here, and also in next section, new parameters are introduced with the essential aim of analyzing physically relevant problems. Since cosmic gravitational waves may significantly contribute to the CMB angular power spectrum for  $\ell \lesssim 100$ , and the most important deviations between the VT and GR temperature multipoles just arise for these  $\ell$  values, some differences between the GR and VT parameters  $r_{0.05}$  and  $r_{0.002}$  seem to be possible and, consequently, our attention is now focused on the Planck+WP-TM fit, which includes tensor modes.

GR ( $D = 0$ ) and VT ( $D \neq 0$ ) results may be compared by using Table 4 and figures 3-5. In this Table, columns 3-7 show quantities as those of Tables 1- 3, but calculated at  $2\sigma$  confidence level (probability around 95%). This choice allow us to compare our results with those of [13].

In the fit of this section, which includes tensor modes, the  $2\sigma$  upper limit of  $D \times 10^{-8}$  -displayed in Table 4- is 3.665, whereas in the Planck-WP fit, the corresponding  $2\sigma$  limit is 3.894; hence, this limit is only weakly influenced by tensor modes. This is consistent with the right panel of figures 3, where we see that the solid line (Planck+WP) is a little wider than the dashed curve (Planck+WP-TM). Moreover, tensor modes have reduced the best fit value of  $D$  (compare Tables 1 and 4), although it is not highly significant. Parameters  $r_{0.05}$  (adjusted) and  $r_{0.002}$  (derived) deserve attention. As it follows from the last row of Table 4, the relative deviation -between VT and GR- corresponding to  $r_{0.002}$  is  $\Delta(U2) \simeq -6.20\%$  and the  $2\sigma$  upper limit in VT is  $U2 \simeq 0.1086$ ; hence, the  $2\sigma$  upper limit in GR is found to be  $U2 \simeq 0.11554$  and, consequently, we can write:

$$r_{0.002} < 0.1086 \text{ (VT, } \simeq 95\%)$$

and

$$r_{0.002} < 0.11554 \text{ (GR, } \simeq 95\%).$$

This last inequality is to be compared with eq. (63a) in [13], where one can read  $r_{0.002} < 0.11$  ( $\simeq 95\%$ ) for a Planck+WP+highL-TM fit -in GR- performed with the original CAMB and COSMOMC codes. In practice, these two bounds are almost equivalent. The first of the above inequalities (VT) is also very similar to that of (GR). All this is in agreement

**Table 4.** Planck+WP-TM fit

Parameter	BF	L2	U2	$\Delta(L2)$	$\Delta(U2)$	R2
$D \times 10^{-8}$	0.783	0.000	3.6655	-	-	-
$\Omega_b h^2$	0.02219	0.02154	0.02265	-0.37%	0.27%	1.144
$\Omega_c h^2$	0.1186	0.1139	0.1244	-1.48%	1.62%	1.544
$100\theta_{MC}$	1.0417	1.0401	1.0429	-0.01%	0.04%	1.217
$\ln(10^{10} A_s)$	3.080	3.038	3.136	-0.03%	0.00%	1.010
$n_s$	0.9629	0.9480	0.9777	-0.32%	0.39%	1.297
$\tau$	0.0847	0.0645	0.1157	-1.54%	0.87%	1.041
$r_{0.05}$	0.0325	0.0000	0.11588	-	-6.20%	0.940
$\Omega_\Lambda$	0.700	0.662	0.726	-2.05%	1.39%	1.588
$\Omega_m$	0.300	0.274	0.338	-3.58%	4.13%	1.588
$\sigma_8$	0.835	0.814	0.864	-0.32%	0.29%	1.112
$z_{re}$	10.57	8.80	13.11	-0.68%	0.23%	1.021
$H_0$	68.48	65.73	70.54	-1.36%	1.18%	1.562
$Y_P$	0.24490	0.24461	0.24510	-0.02%	0.01%	1.162
$t_0$	13.76	13.68	13.88	-0.22%	0.22%	1.429
$r_{0.002}$	0.00289	0.00000	0.10859	-	-6.20%	0.940

with the right panel of figure 3, where one may see that dashed curve (Planck+WP-TM) is located a little below the solid line (Planck+WP) but very close to it. The remaining adjusted parameters, common to the Planck+WP and Planck+WP-TM fits, do not lead to remarkable news; e.g., the spectral index  $n_s$  is considered in the central panel of figure 4, where we see that the dot-dashed line (Planck+WP-TM) is wider than the solid curve (Planck+WP), which is consistent with the value  $R2 = 1.217$  displayed in Table 4. We have focused our attention on  $n_s$  since this parameter is in the exponent of eq. (3.1) together with the running spectral index, which will be included in next fit. Finally, compare the solid (Planck+WP) and dot-dashed lines (Planck+WP-TM) in the left panel of figure 4] to see that the probability of any  $r$  value is rather similar in GR and VT.

With the three basic parameters studied in the last paragraph, we have built up the pairs  $(D \times 10^{-8}, n_s)$  and  $(D \times 10^{-8}, r_{0.002})$ , whose marginalized distribution functions are displayed in figure 5. Since parameter  $D$  vanishes in GR, only VT contours are shown (black curves). These contours confirm (see above) that, at  $1\sigma$  level, one satisfies  $|D| \times 10^{-8} \lesssim 3$ , showing also  $D$  upper limits for  $2\sigma$  and  $3\sigma$  confidence levels.

#### 4.5 Planck+WP-TM-RSI

In the context of GR-CM, it has been proved that a running spectral index strongly modifies the  $r_{0.002}$  upper bound [13] and, on account of this fact, we have studied the Planck+WP-TM-RSI fit. GR and VT results may be compared by using Table 5, which has the same structure as Table 4, and figures 3-4 and 6-7.

As it is seen in Table 5, for the Planck+WP-TM-RSI fit, the  $2\sigma$  VT upper limit of  $D \times 10^{-8}$  is 5.442 and the best fit of this parameter is 1.116; hence, the existence of a nonvanishing parameter  $dn_s/d(\ln k)$  has led to values of both the best fit and the  $2\sigma$  upper limit greater than those of the Planck+WP-TM fit. A greater upper limit (BF value) is consistent with the fact that the dot-dashed line in the right panel of figure 3 is rather wider (has a wider flat central part) than the dashed one.

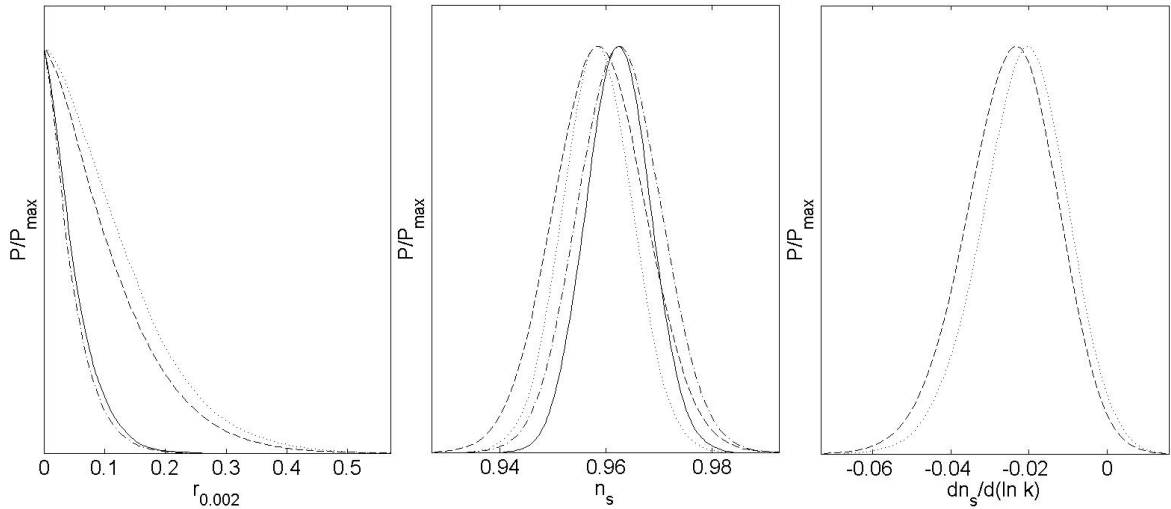


**Figure 4.** Marginalized distribution functions normalized to unity. In all panels, the solid and dot-dashed (dotted and dashed) lines correspond to the Planck-WP-TM (Planck-WP-TM-RSI) fit. Dashed and dot-dashed (dotted and solid) curves are obtained in VT-CM (GR-CM). Each panel shows  $P/P_{max}$  for the parameter specified below the horizontal axis.

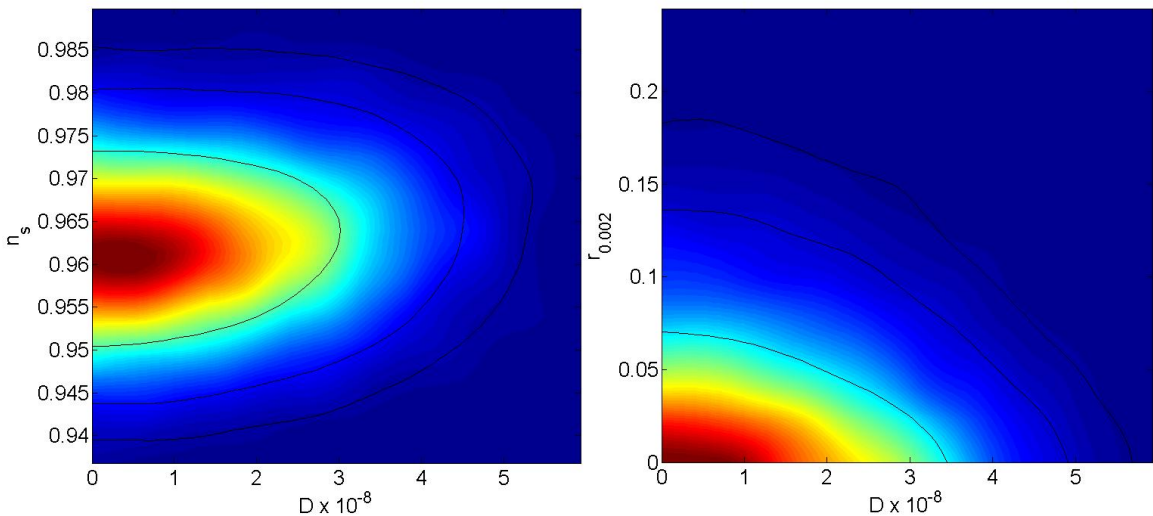


**Figure 5.** Marginalized distribution functions (color), in the Planck+WP-TM fit. Two pairs involving  $D \times 10^{-8}$ , one with  $n_s$  [left] and the other with  $r_{0.002}$  [right], are considered. Contours correspond to the  $1\sigma$  (inner),  $2\sigma$  (middle) and  $3\sigma$  (outer) confidence levels in VT.

Let us now consider parameter  $r_{0.002}$ . In the last row of Table 5, the relative deviation corresponding to this parameter is  $\Delta(U2) \simeq -7.22\%$  and the  $2\sigma$  upper limit in VT is  $U2 \simeq 0.2574$ . The corresponding GR limit is then  $U2 \simeq 0.2767$  and, consequently, for the Planck+WP-TM-RSI fit, one has:

$$r_{0.002} < 0.2574 \text{ (VT, } \simeq 95\%)$$



**Table 5.** Planck+WP-TM-RSI fit

Parameter	BF	L2	U2	$\Delta(L2)$	$\Delta(U2)$	R2
$D \times 10^{-8}$	1.116	0.000	5.442	-	-	-
$\Omega_b h^2$	0.02224	0.02175	0.02304	-0.28%	0.52%	1.162
$\Omega_c h^2$	0.1198	0.1139	0.1250	-1.74%	1.78%	1.609
$100\theta_{MC}$	1.0411	1.0402	1.0427	-0.01%	0.02%	1.136
$\ln(10^{10} A_s)$	3.112	3.054	3.182	-0.07%	0.06%	1.032
$n_s$	0.9611	0.9426	0.9757	-0.36%	0.48%	1.324
$\tau$	0.0992	0.0700	0.1344	-3.23%	1.05%	1.061
$r_{0.05}$	0.0125	0.0000	0.02227	-	-7.39%	0.929
$dn_s/d(\ln k)$	-0.0098	-0.0482	-0.0021	8.55%	51.67%	1.072
$\Omega_\Lambda$	0.692	0.660	0.728	-2.13%	1.68%	1.643
$\Omega_m$	0.308	0.272	0.340	-4.35%	4.27%	1.643
$\sigma_8$	0.849	0.818	0.874	-0.20%	0.16%	1.057
$z_{re}$	11.82	9.50	14.46	0.44%	0.54%	1.007
$H_0$	67.90	65.76	70.88	-1.37%	1.46%	1.610
$Y_P$	0.2449	0.2447	0.2453	0.00%	0.04%	1.200
$t_0$	13.78	13.64	13.85	-0.22%	0.14%	1.312
$r_{0.002}$	0.01165	0.00000	0.2574	-	-7.22	0.930

and

$$r_{0.002} < 0.2767 \text{ (GR, } \simeq 95\%).$$

This last relation must be compared with eq. (63b) in [13], which has the form  $r_{0.002} < 0.26$  ( $\simeq 95\%$ ) for a Planck+WP+highL-TM-RSI fit in GR. The small difference between the values 0.26 and 0.2767 may be due to the use of highL data, which are considered only in [13], and also to the convergence criterium which is more severe in our case; in any way, these two values and 0.2574 (VT fit) are too similar to speak about significant differences between GR and VT.

Finally, for the parameter  $dn_s/d(\ln k)$ , we have found  $\Delta(L2) = 8.55\%$  and  $\Delta(U2) = 51.67\%$  (see Table 5). These are the maximum relative deviations between GR and VT arising in this paper. In the same Table, we also see that, for the parameter under consideration and VT, one has  $L2 = -0.0482$  and  $U2 = -0.0021$ . From all these data one easily finds that the corresponding GR values are  $L2 = -0.0442$  and  $U2 = -0.0012$  and, then, one can write:

$$dn_s/d(\ln k) = -0.025 \pm 0.023 \text{ (VT, } \simeq 95\%)$$

and

$$dn_s/d(\ln k) = -0.023 \pm 0.021 \text{ (GR, } \simeq 95\%).$$

In the same way, at  $1\sigma$  confidence, our fit leads to the following relations:

$$dn_s/d(\ln k) = -0.024 \pm 0.012 \text{ (VT, } \simeq 68\%)$$

and

$dn_s/d(\ln k) = -0.021 \pm 0.011$  (GR,  $\simeq 68\%$ ), and this relation is identical to eq. (62a) in [13], which is not surprising at all.

We have focused our attention on parameters  $r_{0.002}$  and  $dn_s/d(\ln k)$ , which are characteristic of the non-minimal fit of this section. Hereafter, parameter  $n_s$  is also considered as it was done in section 4.4. The marginalized distribution functions  $P/P_{max}$  of these three parameters are displayed in figure 4. In the left, central, and right panels, the dotted and dashed lines give  $P/P_{max}$  in the context of GR-CM and VT-CM, respectively. By compar-

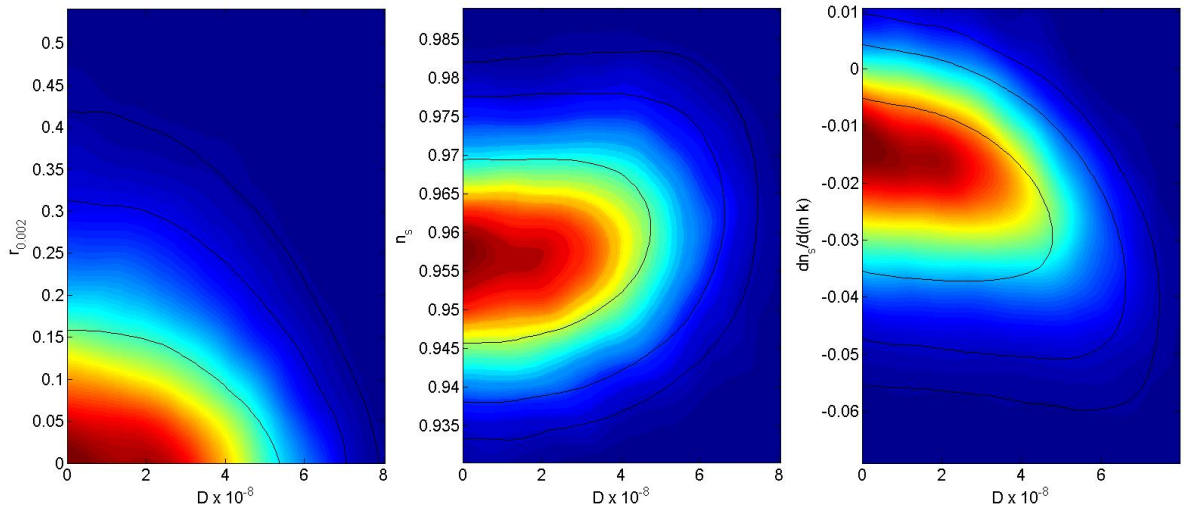


**Figure 6.** Same as in figure 5 for three pairs. Each of them involves  $D \times 10^{-8}$  and other parameter displayed in the vertical axis of the corresponding panel.

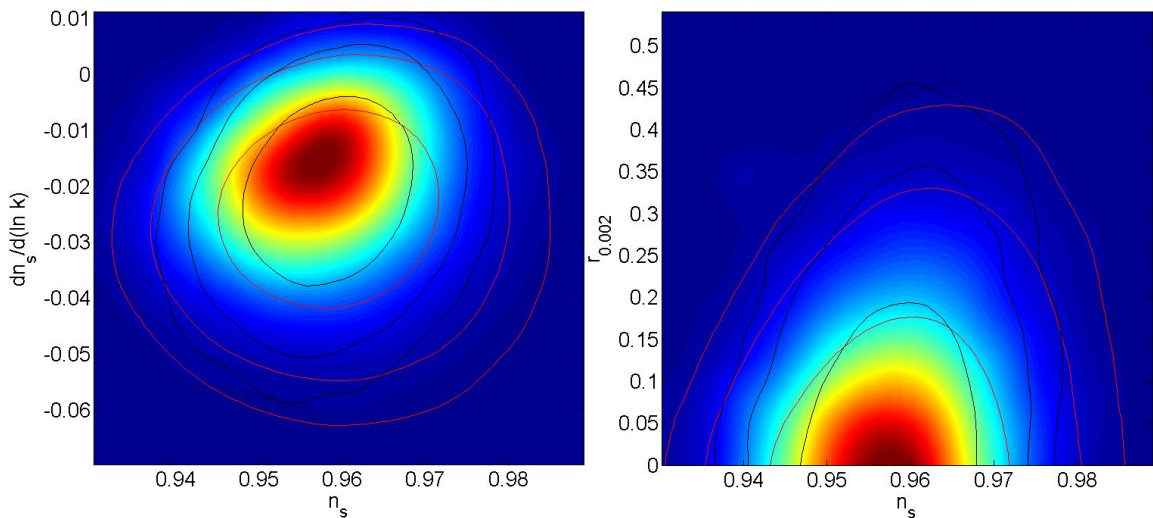


**Figure 7.** Marginalized distribution functions (color) in the Planck+WP-TM-RSI fit for the pairs specified in the panels, in which red [black] contours correspond to the  $1\sigma$  (inner),  $2\sigma$  (middle) and  $3\sigma$  (outer) confidence levels in VT [GR]

ing these two types of lines, one easily concludes that they are rather similar; which means that the introduction of a running spectral index produces similar effects in VT and GR. In both cases, these effects are important as it follows from the comparison of dotted with solid lines (GR) and dashed with dot-dashed curves in the left and central panels, but this importance is rather similar in both theories. All this is in agreement with previous comments and inequalities based on Table 5.

As in section 4.4, let us now show the marginalized distribution function for the same pairs as in figure 5, and also for the new pair  $[D \times 10^{-8}, dn_s/d(\ln k)]$ . The three functions are displayed in figure 6. In the three panels one sees that, if the running spectral index is fitted, the inequality  $|D| \times 10^{-8} \lesssim 5$  is satisfied at the  $1\sigma$  level, with greater upper limits at  $2\sigma$  and  $3\sigma$ . The  $|D|$  upper limits of this section are larger than those of section 4.4 where  $dn_s/d(\ln k) = 0$ , which means that, if the running spectral index is fitted,  $D$  values larger than those of the Planck+WP-TM fit are possible at a given confidence level.

Finally, the marginalized distribution functions of the pairs  $[n_s, dn_s/d(\ln k)]$  and  $[n_s, r_{0.002}]$  are shown in figure 7, where one easily see that the red contours (VT) delimit more extended areas than the black curves (GR) for the same confidence level, which suggests once more that a non vanishing  $D$  parameter facilitates adjustments between theoretical predictions and observational data.

## 5 Discussion and conclusions

Detailed analysis of VT have been developed here and also in [1–4]; so, VT has become one of the best tested gravity theories. Beside the outcomes described in section 1, in this paper, we have proved that VT explains current CMB anisotropy data due to Planck collaboration [13], and other cosmological observations about BAO, SNIa, and so on.

There are parameters as  $\varepsilon$  and  $\gamma$  involved in the action 1.1, which keep almost arbitrary after our exhaustive analysis. Only the inequalities  $\gamma > 0$  and  $2\varepsilon > \gamma$  must be satisfied. The first relation is necessary to have positive dark energy in the cosmological background (with  $W = -1$ ), and the second inequality is necessary to built up a VT theory without classical instabilities and quantum ghosts.

The sign of quantity  $\Xi_B$  -see section 2- remains arbitrary; however, its absolute value is fixed to have an admissible  $A^\mu$  background energy density.

Finally, there is another parameter,  $D$ , whose absolute value  $|D|$  normalizes the spectrum of the scalar  $A^\mu$  cosmological perturbations. The  $|D|$  value control the departures between VT and GR for scalar cosmological perturbations. The sign of  $D$  is irrelevant.

Cosmological parameters, including  $|D|$ , have been numerically estimated for five significant fits involving different observational data. Three of these fits are minimal (seven parameters), whereas other two consider additional parameters to study both inflationary gravitational waves and running spectral indexes. The numerical codes we have used -in VT- are suitable modifications of the well known codes CAMB and COSMOMC. Our results are similar to those obtained by the Planck collaboration in the context of GR [13], but it has been verified that parameter  $|D|$  does not harm the estimation of other parameters involved in the standard cosmological model (GR-CM); on the contrary, if  $D$  is considered as an additional parameter to be adjusted (VT-CM) and a certain confidence level is assumed, we have found that, in VT-CM, most GR parameters belong to intervals wider than those of the GR-CM and, consistently, quantity  $|D|$  takes on non vanishing values. Parameter  $|D|$  plays a positive statistical role in the study of VT scalar perturbations.

New applications or appropriate generalizations of VT could be necessary to fix  $\gamma$ ,  $\varepsilon$  and the sign of  $\Xi_B$ . The new applications should probably be nonlinear as, e.g., the study a binary stellar systems radiating gravitational waves or a deep analysis of the black holes and their surroundings (see [3]). Interesting VT generalizations could be obtained by replacing  $R$  by an appropriated function  $f(R)$  in action 1.1; thus, the field  $A^\mu$  could explain the accelerated late time expansion, whereas the scalar field, associated to  $f(R)$  in the Einstein frame,

could account for the required inflation; hence, function  $f(R)$  would be chosen to achieve a good inflation, without producing late time acceleration, which implies less restrictions to be satisfied by  $f(R)$ . Finally, in appropriate VT generalizations,  $A^\mu$  vector modes might suitably evolve -coupled to other modes of the same type- to explain interesting effects as, e.g., the CMB anomalies observed by WMAP and Planck at very large angular scales [19, 23–26]. This explanation is not easy in the context of GR and VT, where vector modes decay [27, 28]. These promising developments are beyond the scope of this paper.

## Acknowledgments

This work has been supported by the Spanish Ministry of Economía y Competitividad, MICINN-FEDER project FIS2015-64552-P and CONSOLIDER-INGENIO project CSD2010-0064. We thank J.A. Morales-LLadosa for useful discussion. Calculations were carried out at the Centre de càlcul de la Universitat de València.

## References

- [1] R. Dale and D. Sáez, *Cosmological perturbations in extended electromagnetism. General gauge invariant approach*, *Phys. Rev. D* **85** (2012) 124047
- [2] R. Dale and D. Sáez, *Cosmology in a certain vector-tensor theory of gravitation*, *Phys. Rev. D* **89** (2014) 044035
- [3] R. Dale, M.J. Fullana and D. Sáez, *On the horizons in a viable vector-tensor theory of gravitation*, *Ap&SS* **357** (2015) 116
- [4] R. Dale, J.A. Morales and D. Sáez, *Proposal for the origin of the cosmological constant*, arXiv:0906.2085[astro-ph.CO]
- [5] C.M. Will, *Theory and experiment in gravitational physics*, Cambridge University Press, NY (1993)
- [6] C.M. Will, *The confrontation between general relativity and experiments*, *Living Rev. Relativity* **9** (2006) 3
- [7] J. Beltrán Jiménez and A.L. Maroto, *Viability of vector-tensor theories of gravity*, *JCAP* **02** (2009) 025
- [8] A. Lewis, A. Challinor and A. Lasenby, *Efficient computation of cosmic microwave background anisotropy in closed Friedmann Robertson Walker models*, *ApJ* **538** (2000) 473
- [9] J.M. Bardeen, *Gauge-invariant cosmological perturbations*, *Phys. Rev D* **22** (1980) 1882
- [10] W. Hu and M. White, *CMB anisotropies: total angular momentum method*, *Phys. Rev. D* **56** (1997) 596
- [11] C.P. Ma and E. Bertschinger, *Cosmological perturbation theory in the synchronous and conformal Newtonian gauges*, *ApJ*, **455** (1995) 7
- [12] A. Lewis and S. Bridle, *Cosmological parameters from CMB and other data: a Monte Carlo approach*, *Phys. Rev. D* **66** (2002) 103511
- [13] Planck Collaboration, *Planck 2013 results. XVI. Cosmological parameters*, *A&A* **571** (2014) A16
- [14] U. Seljak and M. Zaldarriaga, *A line-of-sight integration approach to cosmic microwave background anisotropies*, *ApJ* **469** (1996) 437
- [15] E.D. Kolb and M.S. Turner, *The early universe*, Addison-Wesley Publishing Company (1994)

- [16] M. Costanzi, B. Sartoris, M. Viel and S. Borgani, *Neutrino constraints: what large-scale structure and CMB data are telling us?*, *JCAP* **10** (2014) 81
- [17] N. Jarosik et al. *Seven-year Wilkinson microwave anisotropy probe (WMAP) observations: sky maps, systematic errors, and basic results*, *ApJS* **192** (2011) 14
- [18] G. Hinshaw, et al., *Nine-year Wilkinson microwave anisotropy probe (WMAP) observations: cosmological parameter results*, *ApJS* **208** (2013) 19
- [19] Planck Collaboration, *Planck 2013 results. I. Overview of products and scientific results*, *A&A* **571** (2014) A1
- [20] Planck Collaboration, *Planck 2015 results. XIII. Cosmological parameters*, *A&A* **594** (2016) A13
- [21] Planck Collaboration, *Planck 2015 results. I. Overview of products and scientific results*, *A&A* **594** (2016) A1
- [22] E. Di Valentino, A. Melchiorri and J. Silk, *Beyond six parameters: Extending  $\Lambda$ CDM*, *Phys. Rev. D* **92** (2015) 121302
- [23] A. de Oliveira-Costa, M. Tegmark, M. Zaldarriaga and A. Hamilton, *Significance of the largest scale CMB fluctuations in WMAP*, *Phys. Rev. D* **69** (2004) 063516
- [24] C.J. Copi, D. Huterer and G.D. Starkman, *Multipole vectors: A new representation of the CMB sky and evidence for statistical anisotropy or non-Gaussianity at  $2 \leq \ell \leq 8$* , *Phys. Rev. D* **70** (2004) 043515
- [25] H.J. Eriksen, F.K. Hansen, A.J. Banday, K.M. Górski and P.B. Lilje, *Asymmetries in the Cosmic Microwave Background Anisotropy Field*, *ApJ* **605** (2004) 14
- [26] F.K. Hansen, A.J. Banday, K.M. Górski and P.B. Lilje, *Asymmetries in the Cosmic Microwave Background Anisotropy Field*, *MNRAS* **354** (2004) 641
- [27] J.A. Morales and D. Sáez, *Evolution of polarization orientations in a flat universe with vector perturbations: CMB and quasistellar objects*, *Phys. Rev. D* **75** (2007) 043011
- [28] J.A. Morales and D. Sáez, *Large-scale vector modes and the first CMB temperature multipoles*, *ApJ* **678** (2008) 583